

# Uniaxially anisotropic antiferromagnets in a field along the easy axis

W. Selke<sup>1</sup>, M. Holschneider<sup>1</sup>, R. Leidl<sup>2</sup>, S. Wessel<sup>3</sup>, and G. Bannasch<sup>1</sup>

<sup>1</sup> Institut für Theoretische Physik, RWTH Aachen, 52056 Aachen, Germany

<sup>2</sup> Department of Physics, Simon Fraser University, Burnaby, British Columbia V5A 1S6, Canada

<sup>3</sup> Institut für Theoretische Physik III, Universität Stuttgart, 70550 Stuttgart, Germany

**Summary.** Uniaxially anisotropic antiferromagnets in a field along the easy axis are studied with the help of ground state considerations and Monte Carlo simulations. For classical models, the XXZ model as well as variants, we analyze the role of non-collinear spin configurations of biconical or bidirectional type interpolating between the well-known antiferromagnetic and spin-flop structures. Possible experimental applications to layered cuprate antiferromagnets are discussed. Finally, results of quantum Monte Carlo simulations for the  $S=1/2$  XXZ model on a square lattice are presented, and compared with previous findings.

## 1 Introduction

Since many years uniaxially anisotropic antiferromagnets in a field have been studied extensively, both experimentally and theoretically. The magnets are

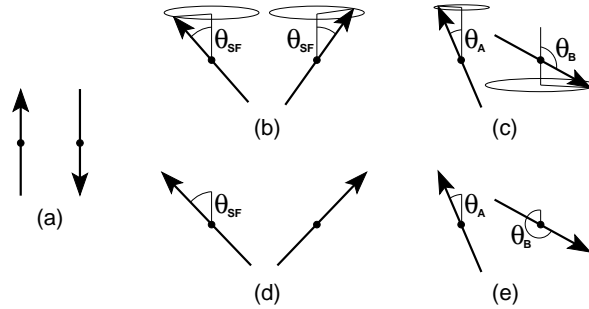


**Fig. 1.** Spin orientations on neighboring sites showing AF (a), SF (b,d), and BC (c) as well as BD (e) ground state structures in XXZ (a,b,c) and anisotropic XY (a,d,e) antiferromagnets.

known to display at low temperatures,  $T$ , upon increasing the field  $H$  along the easy axis, antiferromagnetic (AF) and spin-flop (SF) phases [1]. A prototypical model describing these phases is the XXZ Heisenberg antiferromagnet, with the Hamiltonian

$$\mathcal{H}_{\text{XXZ}} = J \sum_{i,j} [\Delta(S_i^x S_j^x + S_i^y S_j^y) + S_i^z S_j^z] - H \sum_i S_i^z \quad (1)$$

where  $S_i^x$ ,  $S_i^y$ , and  $S_i^z$  denote the spin components at lattice site  $i$ . The first sum runs over pairs of neighboring sites  $(i, j)$  of the square or cubic lattice;  $J > 0$  is the exchange integral, and  $\Delta$ ,  $0 < \Delta < 1$ , determines the strength of the anisotropy along the easy axis ( $z$ -axis). The field  $H$  acts along the  $z$ -axis. Classical XXZ antiferromagnets on square and cubic lattices have been analyzed using Monte Carlo techniques first about three decades ago [2, 3].

Additional phases in the  $(H, T)$ -plane, observed in experiments and theoretical studies, have been attributed to, for instance, further anisotropy terms and/or interactions ranging beyond nearest neighbors [4, 5, 6].

One of the main aims of the present contribution is to draw attention to recent theoretical analyses of the classical XXZ antiferromagnet and its analogue for spins with only two components, the anisotropic XY antiferromagnet [7, 8, 9, 10, 11]. Especially, the importance of non-collinear structures of biconical (BC) or bidirectional (BD) type, see Fig. 1, is emphasized [10, 11, 12]. By adding a single-ion anisotropy term to the XXZ model, these structures may be enhanced or suppressed, depending on whether that term favors a planar or a uniaxial anisotropy [11]. Some of the recent theoretical analyses have been partly motivated by experiments on quasi-two-dimensional cuprate antiferromagnets, the 'telephone number compounds'  $(Ca, La)_{14}Cu_{24}O_{41}$  [13, 14, 15, 16, 17]. Thence, we shall discuss also more complicated models for uniaxially anisotropic two-dimensional antiferromagnets proposed to describe such compounds, in particular  $Ca_5La_9Cu_{24}O_{41}$  (here, one may mention previous and recent experimental studies on related quasi-two-dimensional antiferromagnets [18, 19, 20, 21, 22] as well).

Finally, we shall consider the quantum,  $S = 1/2$ , version of the XXZ antiferromagnet, which is equivalent to a Bose-Hubbard model [23, 24], on a square lattice, being, especially, of current interest in the context of super-solids. The model is simulated using the method of stochastic series expansions (SSE). New results [10] on the phase diagram will be compared with previous ones [24, 25, 26].

Our findings will be summarized at the end of this contribution.

## 2 The classical XXZ Heisenberg antiferromagnet

The classical XXZ Heisenberg antiferromagnet is described by the Hamiltonian given in Eq. (1), where we shall deal with spin vectors of length unity on square and cubic lattices.

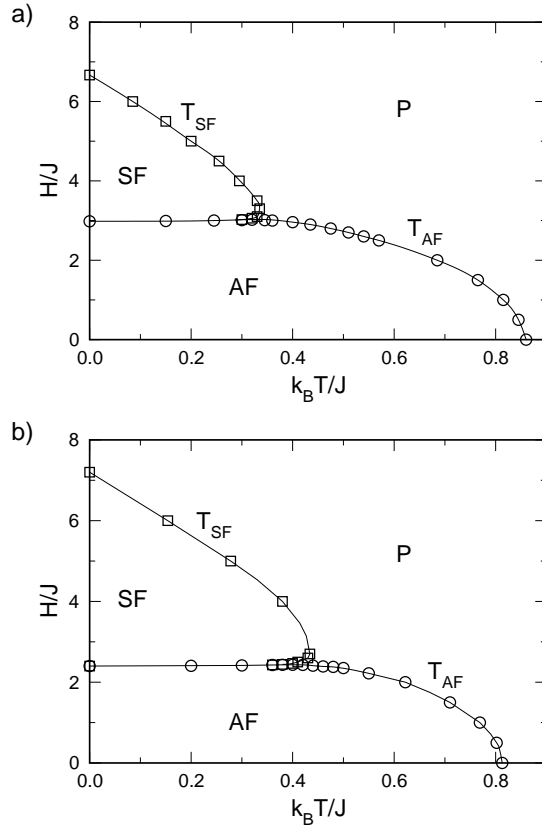


**Fig. 2.** Phase diagram of the classical XXZ model with  $\Delta = 2/3$  (a) and  $4/5$  (b).

We first consider the twodimensional version. Phase diagrams in the  $(T, H)$ -plane are depicted in Fig. 2, where we set the exchange anisotropy  $\Delta$  to be equal to  $2/3$  and  $4/5$ , the latter case being the standard choice [2, 3, 7, 8, 10].

The general topology of the phase diagram seems to be independent of the concrete value of  $\Delta$ ,  $0 < \Delta < 1$ , comprising the long-range ordered AF and the algebraically ordered SF phase. The boundary lines to the disordered phase are in the Ising universality class for the AF case, and in the Kosterlitz–Thouless universality class [27] for the SF case [2, 7]. The AF and SF phase boundary lines approach each other very closely near the maximum of the SF phase boundary in the  $(T, H)$ -plane, see Fig. 3. Accordingly, at low temperatures, there may be either a direct transition between the AF and SF phases, or two separate transitions with an extremely narrow intervening phase may occur.

Indeed, recent simulations suggest a narrow (disordered) phase between the AF and SF phases [7], extending presumably down to zero temperature [8]. The evidence has been provided by determining the universality classes of the

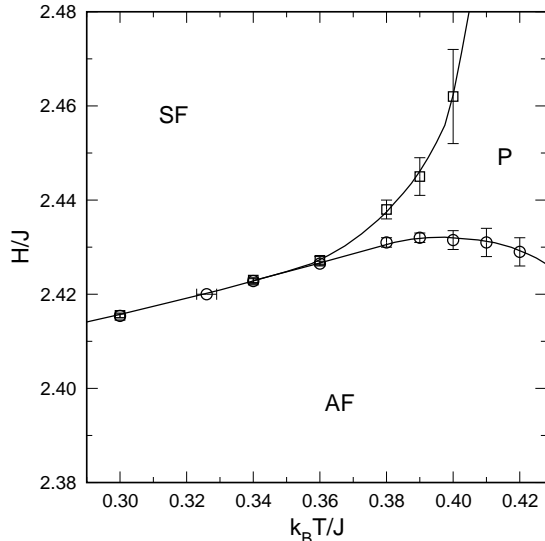


**Fig. 3.** Phase diagram of the classical XXZ model near the maximum of the boundary line of the AF phase,  $\Delta = 4/5$ .

transitions at low temperatures [7, 8], remaining to be of Ising- or Kosterlitz-Thouless type, and by finite-size arguments in the limit of  $T$  approaching zero temperature [8]. The presence of that intervening phase may be argued [10] to be closely related to the highly degenerate ground state occurring at the field  $H_{c1} = 4J\sqrt{1 - \Delta^2}$  separating the AF and SF structures. At that point, not only AF and SF configurations have the same energy, but also biconical structures. Those structures may be described by the tilt angles  $\Theta_A$  and  $\Theta_B$  characterizing the orientations of spin vectors at neighboring sites, belonging to the two different sublattices  $A$  and  $B$ , see Fig. 1. The two tilt angles are interrelated by [10, 11]

$$\Theta_B = \arccos \left( \frac{\sqrt{1 - \Delta^2} - \cos \Theta_A}{1 - \sqrt{1 - \Delta^2} \cos \Theta_A} \right) \quad (2)$$

with the BC configurations interpolating continuously between the AF and SF structures, where the tilt angle  $\Theta_A$  ranges from 0 to  $\pi$ .

The relevance of BC fluctuations in the transition region between the AF and SF phases at low temperatures may be conveniently seen by studying probability functions of the tilt angles, such as the probability  $p_2(\Theta_A, \Theta_B)$  for finding the two angles,  $\Theta_A$  and  $\Theta_B$ , at neighboring sites and the probability  $p(\Theta)$  for encountering the tilt angle  $\Theta$  [10, 11, 12]. An illustration is depicted in Fig. 4, showing that the line of local maxima in  $p_2$  follows closely Eq. (2), signaling that the degenerate BC structures are present in that region. The rather low probability for configurations deviating only slightly from the AF

structure, see Fig. 4, is caused by the small radii of their 'cones'. In fact, at  $T = 0$ , the probability of  $p_2$  along the line given by Eq.(3) is proportional to  $\sqrt{\sin(\Theta_A)\sin(\Theta_B)}$ . In any event, the, presumably, narrow disordered phase seems to be governed by degenerate BC fluctuations, with a hidden 'tetracritical point' at zero temperature [10].

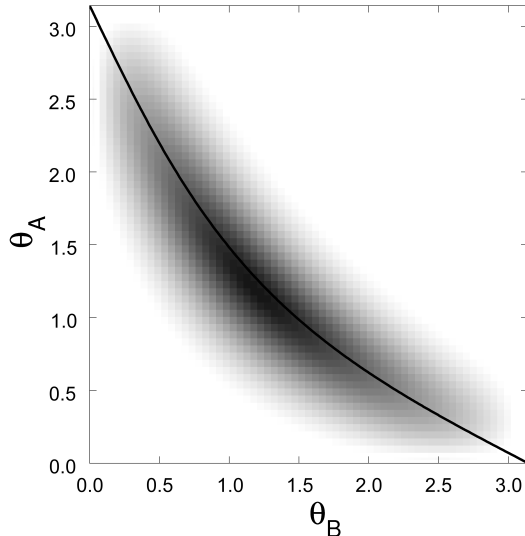


**Fig. 4.** Probability  $p_2(\Theta_A, \Theta_B)$  showing the correlations between the tilt angles  $\Theta_A$  and  $\Theta_B$  on neighboring sites for the XXZ antiferromagnet, with  $80 \times 80$  spins, at  $H/J = 2.41$ ,  $k_B T/J = 0.255$ , and  $\Delta = \frac{4}{5}$ .  $p_2$  is proportional to the gray scale [10]. The superimposed black line depicts the relation between the two angles  $\Theta_A$  and  $\Theta_B$  in the ground state, Eq. (2).

For the classical XXZ antiferromagnet on a cubic lattice early renormalization group arguments [28, 29] and Monte Carlo simulations [3] suggested that the triple point, at which the AF, SF and paramagnetic phases meet, is a bicritical point with  $O(3)$  symmetry (obviously, such a point is excluded to occur, at  $T > 0$ , in two dimensions due to the well-known theorem by Mermin and Wagner [30]). Only a few years ago, this scenario has been questioned, based on high-order perturbative renormalization group calculations [31]. It has been predicted that, instead of the bicritical point, there may be a 'tetracritical biconical' [29] point, due to an intervening ordered 'biconical' phase in between the AF and SF phases, or a point at which first-order transition lines meet.

Our previous Monte Carlo simulations [7] for the three-dimensional XXZ antiferromagnet agreed with a first-order transition between the AF and SF phases at low temperatures. Based on our current simulations [32], again

for  $\Delta = 0.8$ , we locate a triple point at  $k_B T_t/J = 1.025 \pm 0.015$  and  $H_t/J = 3.88 \pm 0.03$ , in reasonable agreement with the estimate by Landau and Binder [3]. So far we did not specify its (multicritical) character. Moreover, we analyzed  $p_2$ , showing that BC fluctuations occur in the transition region between the AF and SF phases temperatures well below  $T_t$ . However, in contrast to the twodimensional case, one now observes a tendency towards coexistence of the AF and SF phases, as reflected by fairly pronounced maxima at the corresponding points in the  $(\Theta_A, \Theta_B)$  plane, compare with Fig. 4. We also estimated critical exponents from monitoring the size dependence of the maxima in the longitudinal, i.e. along the easy axis, as well as the transverse staggered susceptibilities and the specific heat near the transition between the AF and SF phases at temperatures somewhat below that triple point. In agreement with previous findings [3, 7] and the behavior of  $p_2$ , a transition of first order between the AF and SF phases is strongly suggested [32].

### 3 Variants and applications to layered cuprate magnets

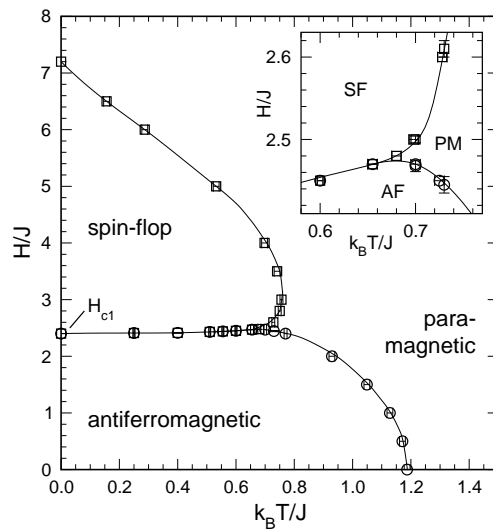


**Fig. 5.** Phase diagram of the anisotropic XY antiferromagnet with  $\Delta = 0.8$ .

In the following, classical variants of the twodimensional XXZ antiferromagnet are studied. From a theoretical point of view, one may like to check the robustness of the topology of the phase diagram against modifying the model, to identify genuine features. From an experimental point of view, one

may like to have a (semi-)quantitative description of measurements. Addressing the first aspect, we added a single-ion anisotropy term to the XXZ model, and we also analyzed the anisotropic XY antiferromagnet on a square lattice. Addressing the experimental aspect, we focused on layered cuprate antiferromagnets, the so-called 'telephone number compounds'  $(Ca, La)_{14}Cu_{24}O_{41}$ , in particular  $Ca_5La_9Cu_{24}O_{41}$ .

### 3.1 Classical anisotropic XY antiferromagnet

Reducing the number of spin components to two and keeping the uniaxial anisotropy, one arrives at the anisotropic XY antiferromagnet, with the Hamiltonian

$$\mathcal{H}_{XY} = J \sum_{i,j} [S_i^x S_j^x + \Delta S_i^y S_j^y] - H \sum_i S_i^x \quad (3)$$

where the  $x$ -axis is now the easy axis. As before,  $0 < \Delta < 1$ . We set  $\Delta = 0.8$ .

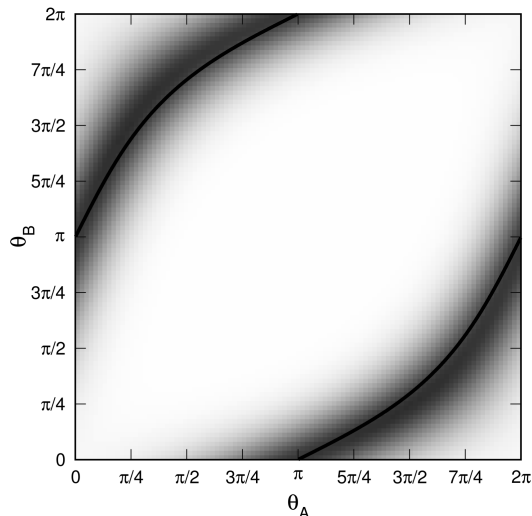


**Fig. 6.** Probability  $p_2(\Theta_A, \Theta_B)$  for the anisotropic XY antiferromagnet with  $\Delta = 0.8$  for a system with  $100 \times 100$  lattice sites in the transition region between the AF and SF phases at  $k_B T/J = 0.558$  and  $H/J = 2.44$ .  $p_2(\Theta_A, \Theta_B)$  is proportional to the grayscale. The superimposed solid line depicts the relation between the two tilt angles  $\Theta_A$  and  $\Theta_B$  in the ground state, see Eq. (2).

The topology of the phase diagram looks like in the XXZ case [11, 12], compare Figs. 2 and 3 with Fig. 5. The AF and SF phase boundary lines approach each other very closely near the maximum of the AF phase boundary

in the  $(T, H)$ -plane. Accordingly, at low temperatures, there seems to be, again, either a direct transition between the AF and SF phases, or two separate transitions with an extremely narrow intervening phase.

In principle, now a bicritical point, with  $O(2)$  symmetry, may occur at non-zero temperature, being of Kosterlitz–Thouless type. Our simulations, however, suggest that, like in the XXZ case, there is a narrow disordered phase intervening between the AF and SF phases down to temperatures well below the point where the AF and SF phases approach each other very closely [11, 12]. In particular, critical exponents of the staggered susceptibilities are found to be compatible with the Ising universality class holding now for the transitions of the AF as well as the SF phases to the disordered phase. The narrow intervening phase seems to be due to degenerate bidirectional structures, see Fig. 1, arising from the highly degenerate ground state at the field  $H_{c1}$ , which separates the AF and SF structures. This behavior is in complete analogy to the one for the XXZ antiferromagnet.

At the highly degenerate ground state, the two tilt angles  $\Theta_A$  and  $\Theta_B$  of the BD structures are interrelated analogously to Eq. (2). In contrast to the XXZ antiferromagnet, however, the probability  $p_2(\Theta_A, \Theta_B)$  along the line of the interrelated tilt angles is now constant at  $T = 0$ . Both properties, the degeneracy and the (almost) constant value of  $p_2$ , tend to hold at low temperatures as well. This is displayed in Fig. 6, depicting  $p_2$  in the transition region between the AF and SF phases at low temperatures.

### 3.2 Adding a single-ion-anisotropy to the XXZ model

The classical XXZ model, Eq. (1), on a square lattice is modified by adding a single-ion anisotropy term of the form

$$\mathcal{H}_{si} = D \sum_i (S_i^z)^2 \quad (4)$$

which either,  $D < 0$ , enhances the uniaxial anisotropy  $\Delta$ , or,  $D > 0$ , may weaken it due to a competing planar anisotropy. The sign of  $D$  will have drastic consequences for the phase diagram [11, 12, 33]. Due to the single-ion term, the highly degenerate ground state, at  $H_{c1}$  in the XXZ model, is removed, suppressing altogether the BC structures, when  $D < 0$ , or spreading them over a finite range of fields, limited by  $H_{c1a}$  and  $H_{c1b}$ , when  $D > 0$ , see Fig. 7.

In the latter case of a competing anisotropy, an ordered BC phase arises at low temperatures, bordered by the AF and SF phases, as shown in Fig. 7. Based on renormalization group calculations [34, 35, 36, 37], the transition between the BC and SF phases may be argued to be in the Ising universality class, while the transition between the BC and AF phases is expected to be in the XY universality class, being the Kosterlitz–Thouless universality class in two dimensions. This description is in accordance with our simulational



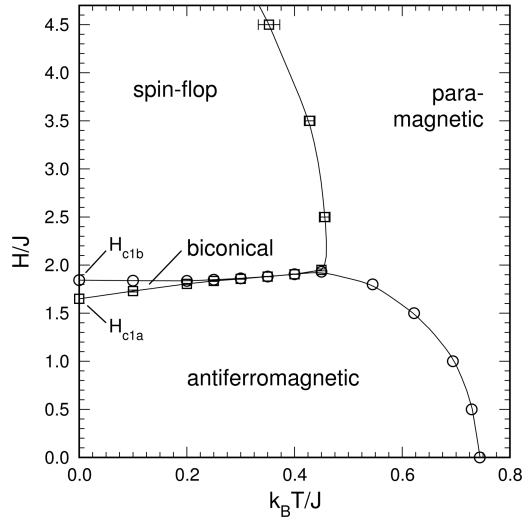


**Fig. 7.** Phase diagram of the XXZ antiferromagnet with a competing single-ion anisotropy,  $\Delta = 0.8$  and  $D/J = 0.2$ .

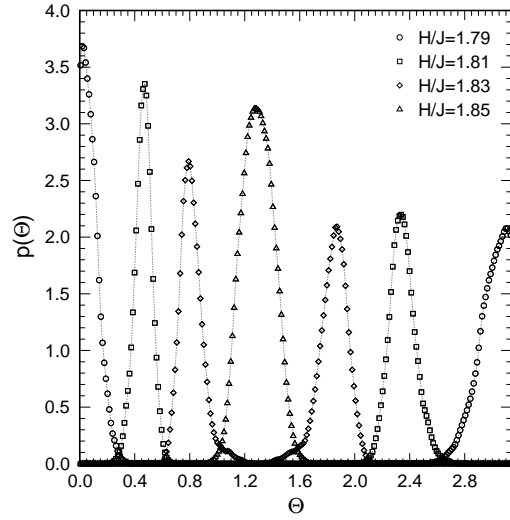


**Fig. 8.** Histograms for the probability of the tilt angle  $p(\theta)$  for the XXZ antiferromagnet with a competing single-ion anisotropy,  $D/J = 0.2$ , at  $k_B T/J = 0.2$ , at the fields given in the inset. Lattices with  $80 \times 80$  spins are simulated.

data, as inferred from critical exponents for staggered susceptibilities and magnetizations at the two different phase boundary lines [11, 12, 33].

In the BC phase the interrelated tilt angles are changing continuously, at fixed low temperature, with the field. This behavior is displayed by the probability function  $p(\Theta)$ , as illustrated in Fig. 8. By increasing the field, the peak positions correspond first to the AF structure, shifting gradually towards each other, reflecting BC structures, and finally merging in one peak characterizing the SF phase.

As seen in Fig. 7, the extent of the BC phase shrinks with increasing temperature. Eventually, the BC phase may terminate at a tetracritical point [5, 34, 35, 36, 37], where the AF, SF, BC, and paramagnetic phases meet [11].

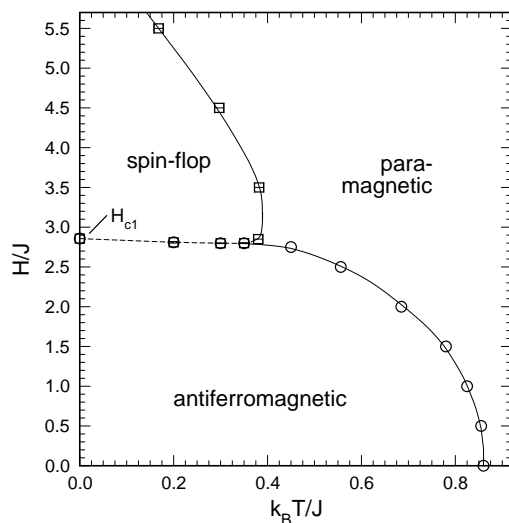


**Fig. 9.** Phase diagram of the XXZ antiferromagnet with a single-ion anisotropy fostering the uniaxiality,  $\Delta = 0.8$  and  $D/J = -0.2$ .

In the case of a negative single-ion anisotropy,  $D < 0$ , enhancing the exchange anisotropy, there are no ground states of BC type. In Fig. 9, a typical phase diagram is depicted, where  $D/J = -0.2$ , showing long-range ordered AF and algebraically ordered SF phases.

At low temperatures, we observe a transition of first order separating the AF and SF phases. Evidence for that kind of transition is provided, especially, by the critical exponent describing the size-dependence of the maximum in the longitudinal staggered susceptibility and by a coexistence phenomenon of AF and SF structures in the transition region between the two ordered phases, showing up, e.g., in  $p(\Theta)$  [11, 12].

When the uniaxiality is solely due to a single-ion anisotropy,  $\Delta = 1, D < 0$ , BC structures do not occur as ground state. Accordingly, one may tend to believe that, at low temperatures, a direct transition of first order between the AF and SF phases takes place, in contrast to a conflicting claim [38]. Of course, this aspect needs to be clarified.

Here, attention is also drawn to interesting recent work on a two-dimensional Heisenberg antiferromagnet with long-range dipolar interactions providing a uniaxial anisotropy [39].

### 3.3 Descriptions related to $Ca_5La_9Cu_{24}O_{41}$

The quasi-two-dimensional uniaxially anisotropic Heisenberg antiferromagnet  $Ca_5La_9Cu_{24}O_{41}$  shows intriguing magnetic features, as the consequence of an interplay of spin and charge properties in the coupled  $CuO_2$  spin chains [13, 40], see below. Perhaps most interestingly, at low temperatures a sharp transition at a fairly low field along the easy axis is followed, at a higher field, by an anomaly in the susceptibility.

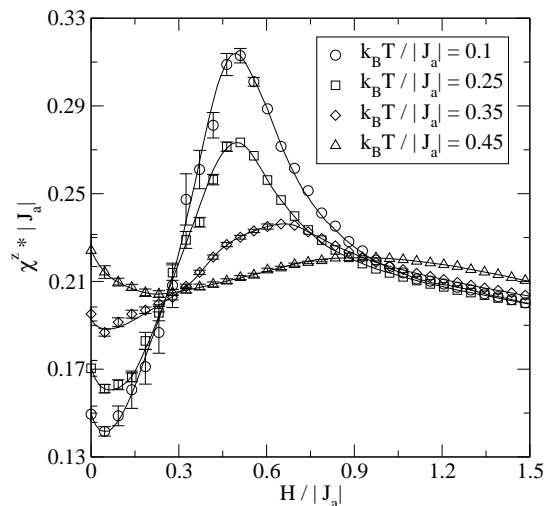


**Fig. 10.** Susceptibility curves for different temperatures as simulated for a two-dimensional uniaxially anisotropic Heisenberg antiferromagnet with quenched defects modeling  $Ca_5La_9Cu_{24}O_{41}$  [17].

To describe the measured spin-wave dispersion of  $Ca_5La_9Cu_{24}O_{41}$  Matsuda *et al.* proposed a classical two-dimensional model with short-range exchange interactions and a single-ion anisotropy [15]. However, the model does not reproduce thermal properties of that magnet like the sharp transition [16, 42]. That transition has been argued to indicate the thermal breaking of

'defect stripes' [13, 40, 41]. The 'defects' correspond to nonmagnetic  $Cu^{3+}$ -ions, due to mobile holes, replacing some of the magnetic  $Cu^{2+}$ -ions in the  $CuO_2$  spin chains (the defect concentration is about 10 percent). Indeed, such a transition has been described by an Ising model with mobile defects [14]. Introducing nonmagnetic, mobile defects in the model of Matsuda *et al.* is, however, not sufficient to reconcile the discrepancy with the measurements [43].

The experimentally observed anomaly at higher fields has been explained qualitatively as indicating the onset of merely *local* spin-flop structures related to a significant decrease in the mobility of the defects or holes [40]. This presumption has been used in a twodimensional uniaxially anisotropic Heisenberg antiferromagnet, with an exchange anisotropy and short-range competing interactions by including defects *quenched* at randomly chosen lattice sites [17]. The model parameters have been carefully chosen, partly on theoretical, partly on experimental grounds. In fact, the model then reproduces (semi-)quantitatively the field dependence of the anomaly when changing the temperature, see Fig. 9. From the simulations, one easily sees that the anomaly is driven by the onset of merely local spin-flop structures, its local character being due to the quenched random defects.

Note that the competing exchange interactions may induce helical spin configurations when tuning the parameters suitably [17].

We should like to mention a recent study on these 'telephone number compounds' applying density functional theory [44], which might also be useful to quantify model parameters.

#### 4 $S = 1/2$ XXZ quantum antiferromagnet on a square lattice

Previous Monte Carlo simulations of the  $S=1/2$  XXZ antiferromagnet on a square lattice suggest that there is, at low temperatures, a direct transition of first order between the AF and SF phases [24, 25, 26].

Schmid *et al.* [24] performed quantum Monte Carlo simulations to determine the phase diagram, for  $\Delta = 2/3$ . They found a topology which resembles that of the classical XXZ antiferromagnet with a negative single-ion anisotropy, compare with Fig. 9. On the boundary line of the AF phase a tricritical point has been reported to occur at  $k_B T_{tc}/J \approx 0.141$ , below which the transition to the paramagnetic phase is of first order. The triple point, at which the AF, SF, and disordered phases meet, is proposed to be a critical endpoint, located at  $k_B T_{ce}/J \approx 0.118$ .

To check these predictions, we performed large scale quantum Monte Carlo simulations [10] using the method of stochastic series expansions with directed loop updates [45]. From those simulations, considering larger system sizes and improved statistics, we conclude that the previous analysis has to be viewed with care. For instance, we studied the model,  $\Delta = 2/3$ , at  $k_B T/J =$

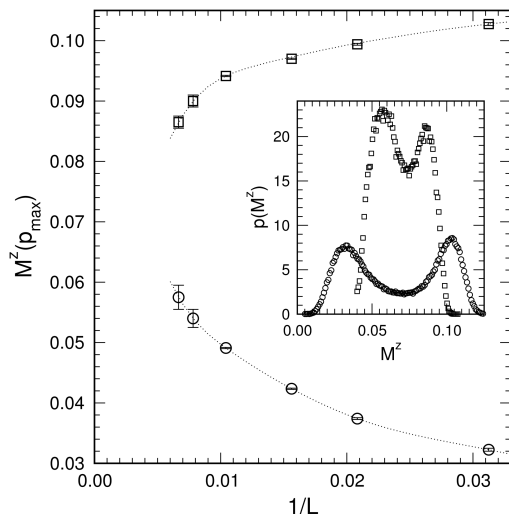


**Fig. 11.** Positions of the maxima of the magnetization histograms as a function of the inverse system size,  $1/L$ , for the  $S=1/2$  XXZ antiferromagnet on a square lattice, with  $\Delta = 2/3$ . The inset exemplifies two histograms for systems of linear size  $L = 32$  (circles) and  $L = 150$  (squares) at  $k_B T/J = 0.13$  and the coexistence fields  $H/J = 1.23075$  and  $H/J = 1.232245$  [10].

0.13, i.e. in between  $T_{tc}$  and  $T_{ce}$ , near the AF phase boundary. In particular, we monitored the size dependence of peak positions in the magnetization histograms, see Fig. 11. Obviously, the two peaks, corresponding to AF and SF structures, may well coincide at the transition in the thermodynamic limit. Thence the transition may well be continuous, in contrast to the previous suggestion. Actually, at the lowest temperature we studied,  $k_B T/J \approx 0.096$ , a continuous transition might still occur [10]. We conclude that the previous [24] scenario with the triple point being a critical endpoint needs to be shifted to somewhat lower temperatures, if it exists at all.

In any event, a clue on possibly distinct phase diagrams for the classical and quantum XXZ antiferromagnets on a square lattice may be the possibly different role of biconical fluctuations. That aspect deserves further studies.

## 5 Summary

In this contribution we presented results of recent Monte Carlo simulations on classical XXZ antiferromagnets in a field along the easy axis as well as classical variants and on the  $S=1/2$  XXZ antiferromagnet on a square lattice.

Basic aspects of phase diagrams and applications to  $Ca_5La_9Cu_{24}O_{41}$  are discussed.

The role of non-collinear structures of biconical and bidirectional type in classical models is emphasized. These structures have an important effect on phase diagrams, in particular, the transition region between the AF and SF phases at low temperatures, and they may provide a clue to explain the possibly different topology of the phase diagrams of classical and quantum,  $S=1/2$ , XXZ antiferromagnets in two dimensions.

We thank especially A. Aharony, K. Binder, B. Büchner, B. Kastening, R. Klingeler, T. Kroll, D. P. Landau, A. Pelissetto, V. L. Pokrovsky, and E. Vicari for cooperation, help, remarks, information, and/or encouragement. Financial support by the Deutsche Forschungsgemeinschaft under grant SE324/4 and by JARA-SIM is gratefully acknowledged.

## References

1. L. Néel, *Ann. Phys.-Paris* **5**, 232 (1936).
2. K. Binder and D. P. Landau, *Phys. Rev. B* **13**, 1140 (1976); D. P. Landau and K. Binder, *Phys. Rev. B* **24**, 1391 (1981).
3. D. P. Landau and K. Binder, *Phys. Rev. B* **17**, 2318 (1978).
4. H. Matsuda and T. Tsuneto, *Prog. Theor. Phys., Supp.* **46**, 411 (1970).
5. K.-S. Liu and M. E. Fisher, *J. Low. Temp. Phys.* **10**, 655 (1973).
6. F. Wegner, *Solid State Commun.* **12**, 785 (1973).
7. M. Holschneider, W. Selke, and R. Leidl, *Phys. Rev. B* **72**, 064443 (2005).
8. C. Zhou, D. P. Landau, and T. C. Schulthess, *Phys. Rev. B* **74**, 064407 (2006).
9. A. Pelissetto and E. Vicari, *Phys. Rev. B* **76**, 024436 (2007).
10. M. Holschneider, S. Wessel, and W. Selke, *Phys. Rev. B* **75**, 224417 (2007).
11. M. Holschneider and W. Selke, *Phys. Rev. B* **76** (R), 024436 (2007).
12. M. Holschneider and W. Selke, *cond-mat/0801.3217*.
13. U. Ammerahl, B. Büchner, C. Kerpen, R. Gross, and A. Revcolevschi, *Phys. Rev. B* **62**, R3592 (2000).
14. W. Selke, V. L. Pokrovsky, B. Büchner, and T. Kroll, *Eur. Phys. J. B* **30**, 83 (2002).
15. M. Matsuda, K. Kakurai, J. E. Lorenzo, L. P. Regnault, A. Hiess, and G. Shirane, *Phys. Rev. B* **68**, 060406(R) (2003).
16. M. Uehara, N. Motoyama, M. Matsuda, H. Eisaki, and J. Akimitsu, in: A. V. Narlikar (Ed.), *Frontiers in Magnetic Materials*, Springer (2005).
17. R. Leidl, R. Klingeler, B. Büchner, M. Holschneider, and W. Selke, *Phys. Rev. B* **73**, 224415 (2006).
18. L. Bevaart, E. Frikkee, and L. J. de Jongh, *Phys. Rev. B* **19**, 4741 (1979).
19. B. D. Gaulin, T. E. Mason, M. F. Collins, and J. Z. Larese, *Phys. Rev. Lett.* **62**, 1380 (1989).
20. R. A. Cowley, A. Aharony, R. J. Birgeneau, R. A. Pelcovits, G. Shirane, and T. R. Thurston, *Z. Phys. B* **93**, 5 (1993).
21. R. J. Christianson, R. L. Leheny, R. J. Birgeneau, and R. W. Erwin, *Phys. Rev. B* **63**, 140401(R) (2001).
22. M. G. Pini, A. Rettori, P. Betti, J. S. Jiang, Y. Ji, S. G. E. te Velthuis, G. P. Felcher, and S. D. Bader, *J. Phys.: Condens. Matter* **19**, 136001 (2007).
23. T. Matsubara and M. Matsuda, *Prog. Theor. Phys.* **16**, 569 (1956).

24. G. Schmid, S. Todo, M. Troyer, and A. Dorneich, *Phys. Rev. Lett.* **88**, 167208 (2002).
25. M. Kohno and M. Takahashi, *Phys. Rev. B* **56**, 3212 (1997).
26. S. Yunoki, *Phys. Rev. B* **65**, 092402 (2002).
27. J. M. Kosterlitz and D. J. Thouless, *J. Phys. C* **6**, 1181 (1973).
28. M. E. Fisher and D. R. Nelson, *Phys. Rev. Lett.* **32**, 1350 (1974).
29. J. M. Kosterlitz, D. R. Nelson, and M. E. Fisher, *Phys. Rev. B* **13**, 412 (1976).
30. N. D. Mermin and H. Wagner, *Phys. Rev. Lett.* **17**, 1133 (1966).
31. P. Calabrese, A. Pelissetto, and E. Vicari, *Phys. Rev. B* **67**, 054505 (2003).
32. G. Bannasch and W. Selke, work in progress.
33. M. Holschneider, PhD thesis, RWTH Aachen (2007).
34. A. D. Bruce and A. Aharony, *Phys. Rev. B* **11**, 478 (1975).
35. A. Aharony, *J. Stat. Phys.* **110**, 659 (2003).
36. D. Mukamel, *Phys. Rev. B* **14**, 1303 (1976).
37. E. Domany and M. E. Fisher, *Phys. Rev. B* **15**, 3510 (1977).
38. R. Costa and W. Pires, *J. Magn. Magn. Mat.* **262**, 316 (2003).
39. C. Zhou, D. P. Landau, and T. C. Schulthess, *Phys. Rev. B* **76**, 024433 (2007).
40. R. Klingeler, PhD thesis, RWTH Aachen (2003).
41. T. Kroll, R. Klingeler, J. Geck, B. Büchner, W. Selke, M. Hücker, and A. Gukasov, *J. Magn. Magn. Mat.* **290**, 306 (2005).
42. R. Leidl and W. Selke, *Phys. Rev. B* **69**, 056401 (2004).
43. R. Leidl and W. Selke, *Phys. Rev. B* **70**, 174425 (2004).
44. U. Schwingenschlögl and C. Schuster, *Europhys. Lett.* **79**, 27003 (2007); *Phys. Rev. Lett.* **99**, 237206 (2007).
45. A. W. Sandvik, *Phys. Rev. B* **59**, R14157 (1999); O. F. Syljuåsen and A. W. Sandvik, *Phys. Rev. E* **66**, 046701 (2002).